Sensors and Actuators B 236 (2016) 719–731

Contents lists available at ScienceDirect

Sensors and Actuators B: Chemical

journal homepage: www.elsevier.com/locate/snb

A new coumarin based dual functional chemosensor for colorimetric detection of Fe^{3+} and fluorescence turn-on response of Zn^{2+}

Nayan Roy, Abhijit Dutta, Paritosh Mondal, Pradip C. Paul, T. Sanjoy Singh*

Department of Chemistry, Assam University, Silchar, Assam 788 011, India

ARTICLE INFO

Article history:
Received 15 December 2015
Received in revised form 23 May 2016
Accepted 9 June 2016
Available online 11 June 2016

Keywords:
Coumarin
Colorimetric sensor
Fluorescence
Selectivity
Logic function
Density functional theory

ABSTRACT

A new coumarin based Schiff-base dual chemosensor-(*E*)-2-(((8-hydroxyquinolin-2-yl)methylene)amino)-6H-benzo[c]chromen-one ($H_{10}L$) was synthesized and characterized. This chemosensor was evaluated as a colorimetric sensor for Fe^{3+} and fluorescence turn-on response for Zn^{2+} among the various survey metal ions. The stoichiometric ratio and association constant were evaluated using Benesi-Hildebrand relation giving 1:1 stoichiometry. This further corroborated 1:1 complex formation based on Job's plot analyses. The complex solution of $H_{10}L$ with Zn^{2+} ion exhibited reversibility with EDTA and regenerate free ligand for further Zn^{2+} sensing. $H_{10}L$ exhibits two INHIBIT logic gates with two different chemical inputs (i) Zn^{2+} (IN1) and Cu^{2+} (IN2) and (ii) Zn^{2+} (IN1) and EDTA (IN2) and the emission as an output. Again, an IMPLICATION logic gate is obtained with Cu^{2+} and EDTA as chemical inputs and emission as output mode. Both free ligand as well as metal-complexes was optimised using density functional theory. The calculated vibrational frequency confirms that both are at local minima on the potential energy surfaces. The corresponding energy difference between HOMO and LUMO of $H_{10}L$, Zn-complex and Cu-complex are found to be 3.67, 1.63 and 2.01 eV, respectively. The Cu-complex is found to be more stable than Zn-complex as Cu-complex has higher hardness value compare to Zn-complex.

1. Introduction

In recent years, more and more attentions have been drawn to devise ingenious fluorescent sensors capable of selective recognition and effectively detecting the presence of alkali, alkaline earth and transition metal ions because of their importance in biological systems as well as to environmental concerned [1,2]. However, among different chemosensors, colorimetric and fluorescence methods based ones have more advantages as they are usually very sensitive, low cost, easily performed and versatile, offering subnanometer spatial resolution with submicron visualisation and submillisecond temporal resolution [3,4]. Nowadays, among the different analyte, special interest is devoted to develop chemosensors for transition metal ions: usually they represent an environmental concern when present in uncontrolled amounts, but at the same time some of them such as iron, zinc, manganese, copper and cobalt are present as essential elements in biological systems. Among biologically important metal ions, iron and zinc cations are the most two abundant and essential trace elements in the human body which play important roles in biology, chemistry and environment. Iron is the most abundant transition metal ion present in the human body. Fe^{3+} ion is an important and essential for proper functioning of all living cells and acts as a cofactor in many enzymatic reactions to human as well as in specialized transport and storage of proteins [5]. The deficiency of Fe^{3+} causes anaemia, liver damage, diabetes, hemochromatosis, Parkinson's disease and cancer [6]. On the other side, zinc is the second most abundant transition metal ion in the human body after iron, and plays a myriad of roles in numerous cellular functions such as regulation of gene expression, apoptosis, co-factors in metalloenzyme catalysis and neurotransmission in biological systems [7,8]. Many severe neurological diseases, including Alzheimer's disease, cerebral ischemia and epilepsy [9–11] are associated with the disorder of Zn^{2+} metabolism. Therefore, estimation of Zn^{2+} is very important in neurobiology. However, there is a great need for developing Zn^{2+} selective sensors that can distinguish Zn^{2+} from other transition metal ions especially Cd^{2+}, because they have very similar chemical properties often respond together with similar spectral changes. However, if unregulated, Fe^{3+} and Zn^{2+} may cause many severe diseases, such as β-thalassemia, Friedreich's ataxia, Alzheimer's disease, Parkinson's disease and epilepsy [12]. There-

* Corresponding author.
E-mail addresses: takhelsingh@gmail.com, singhsanjoy2002@yahoo.co.in (T.S. Singh).

http://dx.doi.org/10.1016/j.snb.2016.06.061
0925-4005/

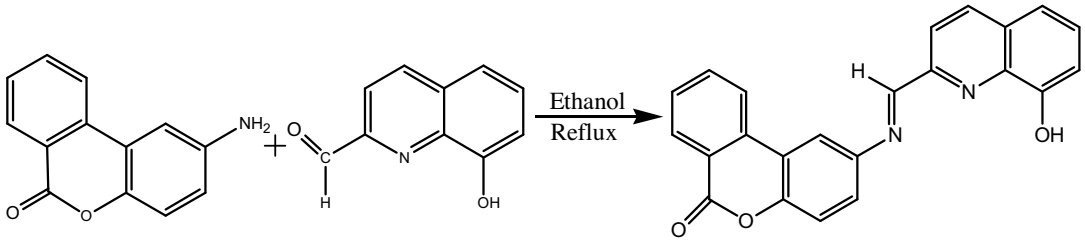

6-amino-3,4-benzocoumarin 8-hydroxyquinoline -2-carbaldehyde

(*E*)-2-(((8-hydroxyquinolin-2-yl)methylene)amino)-6*H*-benzo[*c*]chromen-6-one

Scheme 1. Reaction scheme for the synthesis of (*E*)-2-(((8-hydroxyquinolin-2-yl)methylene) amino)-6H-benzo[c]chromen-6-one ($\mathbf{H_{10}L}$).

fore, there is a great need for developing Zn^{2+} and Fe^{3+} selective sensors that can distinguish Zn^{2+} and Fe^{3+} from other transition metal ions. Many sensors reports are available for detection of both Fe and Zn with synthetic difficulties which require laborious multistep organic synthesis. However, despite much attention of colorimetric as well as fluorescent sensors for selective and sensitive detection of both Fe^{3+} and Zn^{2+}, there is still a huge demand for new sensors with improved properties, especially colorimetric sensors that can make naked eye detection in the visible wavelength, low-cost, requirement of less labour and efficient sensors. Thus the development of dual chemosensors for selective and sensitive detection of trace elements still remains a challenge and active field of research.

Research on molecular logic gates has focussed mainly in the field of chemistry research for its application in information technology since the first AND logic gate was mimicked with optical signals [13]. Various chemical systems have been developed to exhibit different operations like AND, OR, NOT and their integrated operations [14]. In addition, many useful integrated logic gates such as INHIBIT, half subtractor, half adder, full adder, and full subtractor with various single molecules have been exploited [15]. However, during literature surveys, very few IMPLICATION logic gate are reported so far [16]. Recently, there has been reported several molecular logic gates based on the structure of salicylidine Schiff base [17,18]. Some of the coumarin Schiff base was also reported as molecular switch for dual sensing of different metal ions [19].

We know that crown ethers [20], calixarenes [21], porphyrin [22] has been using as an ion-selective electrode for selectively sensing specific metal ions. These compounds have the ability to encapsulate different metal ions depending on their cavity size matching with metal ion diameter. The choice of using nitrogen or sulfur containing crown ethers for better complexation with transition metal ions rather than other survey metal ions has been well established. Again, many drug-based potentiometric membrane sensors based on alcohol, alkaloids, amino acids, vitamins, antibiotics etc. for pharmaceutical analysis in medicinal chemistry [23] and many more for capable of detecting toxic heavy metal ions in environmental samples [24] were also reported. Moreover, few novel metal ions selective sensors like 14 membered N_4 macrocycle [25] for Ni^{2+}, Dimethyl 4, 4′-(o-phenylene)bis(3-thioallophanate) [26] for Cu^{2+}, Morin [27] for Al^{3+}, 2-phenyl-1,3-bis[3′-aza-4′-(2′-hydroxy phenyl)-prop-4-en-1′-yl]-1,3-imidazolidine [28] for Fe^{3+}, 2-hydroxyacetophenoneoxime-thiourea-trioxane resin [29] for UO_2^{2+}, butane-2,3-dione,bis[(2,4-dinitrophenyl)hydrazone [30] for acetate were also found to be reported in the literature. Recently, an analytical application for determination of different metal ions present in drinking water and wastewater over the concern of human health is a challenging task. So, development of less expensive sensors using multi-walled carbon nanotubes-ionic liquid [31] and 8,9-dihydroxy-7-methyl-12H-benzothiazolo[2,3-b]quinazolin [32] modified carbon paste electrode for easy detection of harmful metal ions like Hg^{2+} and hydroxylamine in the presence of phenol and sulphite in different water samples were reported. So, among various analytical methods available, the development of chemical sensors has attained its achievement due to selectivity, non-destructive and low-cost method of analysis. The nitrogen atom of azomethine C=N double bond in Schiff base also exhibits a strong affinity for transition metal ions. Therefore, the Schiff base are known to be good ligand for metal ions [33,34] and used to develop chemosensors. Schiff base metal complexes have numerous applications like antitumor properties [35], antioxidative activities [36], and attractive electronic and photophysical properties [37]. In addition, Schiff base derivatives incorporating a fluorescent moiety are appealing tools for optical sensing of metal ions. Nowadays, designing and synthesis of fluorescent sensors with high selectivity and sensitivity to metal ions is an important and vibrant field. Having much availability of commercial metal ions sensors, chemists still continue endeavouring to design new ones to improve their sensitivity, selectivity and reliability in order to satisfy various needs that are due to the wide existence of metal ions in organisms and its extensive significance. Many excellent metal ions sensors have been contributed significantly but some of the reported synthesis methods are always too complicated. However, only a few coumarin based chemosensors are reported so far for the dual sensing of metal ions [38,39]. As it is well known that coumarin framework exhibits various interesting photophysical properties such as large Stokes shift with visible excitation and emission wavelengths, high quantum yields, good photostability and also has wide application as fluorescent dyes [40–42]. Moreover in the literature, only few coumarin based Schiff base were reported and known to selectively recognize for dual sensing of metal ions [19,43,44]. So, in this paper, we have designed and synthesized a new coumarin based Schiff base dual chemosensor-(*E*)-2-(((8-hydroxyquinolin-2-yl)methylene)amino)-6H-benzo[c]chromen-one ($\mathbf{H_{10}L}$) by one step condensation of 6 amino-3,4-benzocoumarin and 8-hydroxy quinolone-2-carboxaldehyde in ethanol solution (Scheme 1) which selectively and sensitively recognized both Fe^{3+} and Zn^{2+}. The purity of this chemosensor was further characterized by FT-IR, ^1H and ^{13}C NMR and elemental analysis. Herein, the photophysical properties of $\mathbf{H_{10}L}$ were studied in presence of different metal ions, focussing the attention on their absorption and emission properties using steady state absorption and fluorescence spectroscopy. In the UV–vis absorption studies, a strong absorption band at 265 nm, 292 nm and 360 nm were observed in DMF. On addition of Fe^{3+}, the absorption intensity was found to increase with a dramatic change in color which can be easily detected with naked eye. This clearly indicates that $\mathbf{H_{10}L}$ is a highly selective colorimetric sensor for Fe^{3+} ions. In the corresponding absorption spectrum in presence of Fe^{3+}, a strong and broad new absorption band at

320 nm was obtained while the peak at 292 nm disappeared. We also observed a pronounced fluorescence enhancement in presence of Zn^{2+}, while there was no change or minimal spectral changes in presence of other metal ions. This chemosensor was used as a naked eye fluorescent "turn on" detector of Zn^{2+} ion. Importantly, it was able to distinguish Zn^{2+} from Cd^{2+} besides having very similar chemical properties often respond together with similar spectral changes. Moreover, the fluorescence emission behavior of $\mathbf{H_{10}L}$ can be utilised to study as a binary logic function comprising of two INHIBIT logic gates with two different chemical inputs (i) Zn^{2+} (IN1) and Cu^{2+} (IN2) and (ii) Zn^{2+} (IN1) and EDTA (IN2) and the emission as output.

Moreover, full geometry optimization of $\mathbf{H_{10}L}$, $\mathbf{H_{10}L}$-Zn^{2+} and $\mathbf{H_{10}L}$-Cu^{2+} complexes has been carried out using GAUSSIAN 09 program package which suggests the optimized geometry represents stable structures (local minima) in the potential energy surfaces. The corresponding energy difference between HOMO and LUMO of $\mathbf{H_{10}L}$, $\mathbf{H_{10}L}$-Zn^{2+} and $\mathbf{H_{10}L}$-Cu^{2+} complexes are found to be 3.67, 1.63 and 2.01 eV, respectively. The Cu-complex is found to be more stable than Zn-complex as Cu-complex has higher hardness value than Zn-complex.

2. Experimental

2.1. Materials and reagents

6-amino-3, 4-benzocoumarin and 8-hydroxyquinoline-2-carbaldehyde were obtained from Sigma-Aldrich Chemical Company. All the spectroscopic grade solvents used were obtained from Sisco Research Laboratory (SRL) Pvt. Ltd and in some cases, from Sigma-Aldrich Chemical Company. Chemical reagents obtained from Lancaster as well as S.D. Fine Chemical Ltd were of high purity and used without further purification. The solutions of the metal ions were prepared from their perchlorate salts, except for K^+ and Sr^{2+} which was available as KNO_3 and $Sr(NO_3)_2$. All experimental solutions of varying pH were made with phosphate buffer. pH adjustment were done with dilute HCl and NaOH. All experiments were carried out at room temperature (298 K).

2.2. Synthesis and characterization

$\mathbf{H_{10}L}$ was synthesized by condensation of 6-amino-3,4-benzocoumarin and 8-hydroxyquinoline-2-carbaldehyde. A portion of the 6-amino-3,4-benzocoumarin (0.100 g, 0.473 mmol) and 8-hydroxyquinoline-2-carbaldehyde (0.081 g,0.473 mmol) were separately dissolved in absolute ethanol and were combined together to get to yellow color. The solution was refluxed for 3 h in presence of 2–3 drops of acetic acid, and precipitate was filtrated, washed with cold absolute ethanol three times, then recrystallized with ethanol/chloroform (1/3, v/v) to get deep yellow microcrystal in 80% yield. m.p. 147 °C. FT-IR (max, cm^{-1}, KBr): 3377(OH), 3192(as(C—H), 3047(s(C—H),), 1596(C=N), 1572(C=C), 1240((C—O)), 1128((C—N)), 787((C—H)); ^{1}H NMR (400 MHz, DMSO-d_6, TMS, δ, ppm): 7.61 (d, H-1), 8.1 (t, H-2), 7.3 (d, H-3), 7.6 (d, H-4), 8.6 (d, H5),7.79 (d, H-6), 7.65 (s, H-7), 7.87(t, H-8), 8.44 (t, H-9), 8.79 (d, H-10); ^{13}C NMR (400 MHz, DMSO-d_6, TMS, δ, ppm):112.2, 117.9,120.1, 120.4, 121.0, 122.0, 123.4, 126.6, 126.9, 127.5, 128.9, 130.8, 131.9, 134.2, 134.4, 136.1, 137.5, 146.3, 149.6, 150.0, 151.7, 153.2, 158.5; Anal. Calc. for $C_{23}H_{14}N_2O_3$ (366.1): C, 75.4%; H, 3.85%; N, 7.65%. Found: C, 74.8%; H, 3.89%; N, 7.25%. ESI–MS, *m/z*: Calcd for $C_{23}H_{14}N_2O_3$ $(M+H)^+$: 367.1, found: 367.0.

2.3. Instruments

The Infrared spectra were measured on a PerkinElmer L 120-000A spectrophotometer with KBr pellets in the range 4000–400 cm^{-1}. ^{1}H and ^{13}C NMR spectra were recorded on Varian, Mercury Plus–400 MHz spectrometer with chemical shifts reported as ppm (in DMSO-d_6, tetramethylsilane as internal standard). Mass spectra were recorded on Waters, Q-ToF Premier, Mass spectrometer. Elemental analyses were carried out using PE2400 elemental analyser. All pH value was measured with Global Digital pH meter (DPH-500).

Steady state absorption spectra were recorded on a Shimadzu UV-1601PC absorption spectrophotometer and fluorescence emission spectra in PerkinElmer LS 45 fluorescence spectrophotometer. In both fluorescence emission and excitation spectra measurements, 5 nm bandpass was used in the excitation and emission side. Fluorescence quantum yields (ϕ_f) were calculated by comparing the total fluorescence intensity under the whole fluorescence spectral range with that of a standard ($\phi_f = 0.546$, quinine sulfate in 1 M sulphuric acid) using the following equation [45].

$$\phi_f^i = \phi_f^s \times \frac{F^i}{F^s} \times \frac{1-10^{-A^s}}{1-10^{-A^i}} \times \left(\frac{\eta^i}{\eta^s}\right)^2 \quad (1)$$

where F is the total fluorescence intensity under whole fluorescence spectral curve, A^i and A^s is the optical density of the sample and standard, respectively and η^i is the refractive index of the solvent at 298 K.

Fluorescence lifetimes were determined in a nano-LED based time-resolved fluorimeter obtained from Photo Technology International (PTI) using TCSPC technique. The instrument response function (IRF) was obtained at 360 nm using a dilute colloidal suspension of dried non-dairy coffee whitener. The half width of the IRF was ~100 ps. The samples were excited at 360 nm and the fluorescence emission was collected at corresponding emission wavelength. The number of counts in the peak channel was at least 10000. In fluorescence lifetime measurements, the emission was monitored at the magic angle (54.7°) to eliminate the contribution from the decay of anisotropy.

Density functional theory (DFT) calculation is performed to investigate the electronic structure of $\mathbf{H_{10}L}$, $H_{10}L$-Zn^{2+} and $H_{10}L$-Cu^{2+} complexes using GAUSSIAN 09 program package. Full geometry optimization of $\mathbf{H_{10}L}$ and metal-complexes has been carried out without imposing any constrain using Becke's [46] three parameter hybrid exchange functional (B3) and the Lee-Yang-Parr correlation functional (LYP) (B3LYP) [47] along with 6–31G** [48] basis set. In order to confirm the stability of $\mathbf{H_{10}L}$ and metal-complexes, we performed vibrational frequency calculations at the same level of theory.

3. Results and discussion

3.1. UV–vis titration studies

The absorption spectrum of $\mathbf{H_{10}L}$ shows a strong absorption band at 265 nm, 292 nm and 360 nm in DMF (Fig. 1). The recognition profiles of $\mathbf{H_{10}L}$ towards different metal cations like alkali (Na^+, K^+), alkaline earth (Ca^{2+}, Mg^{2+}, Sr^{2+}) and transition metal ions (Cd^{2+}, Ni^{2+}, Co^{2+}, Cu^{2+}, Zn^{2+} and Fe^{3+}) were primarily investigated by absorption spectroscopy in DMF. On addition of Fe^{3+}, the absorption intensity was found to increase with a dramatic change in color, from colorless to deep yellow, which can be easily detected with naked eye. However, in presence of other metal ions, there is no change in the absorption intensity which clearly indicates that $\mathbf{H_{10}L}$ is a highly selective colorimetric sensor for Fe^{3+} ions. In the corresponding absorption spectrum in presence of Fe^{3+}, the peak at 292 nm was disappeared and a strong and broad new absorption band at 320 nm was obtained. To further investigate the interaction between $\mathbf{H_{10}L}$ and Fe^{3+}, UV–vis absorption spectral variation of $\mathbf{H_{10}L}$ (5 μM) in DMF was monitored in presence of different

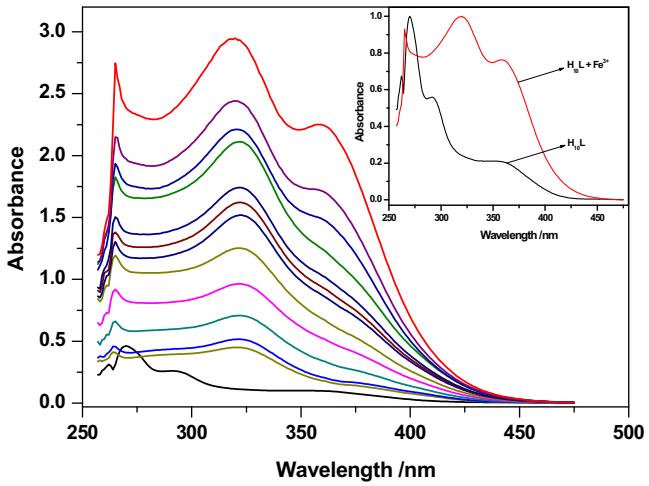

Fig. 1. Change in UV–vis spectrum of $\mathbf{H_{10}L}$ (5 μM) upon gradual addition of Fe^{3+} in DMF at room temperature.

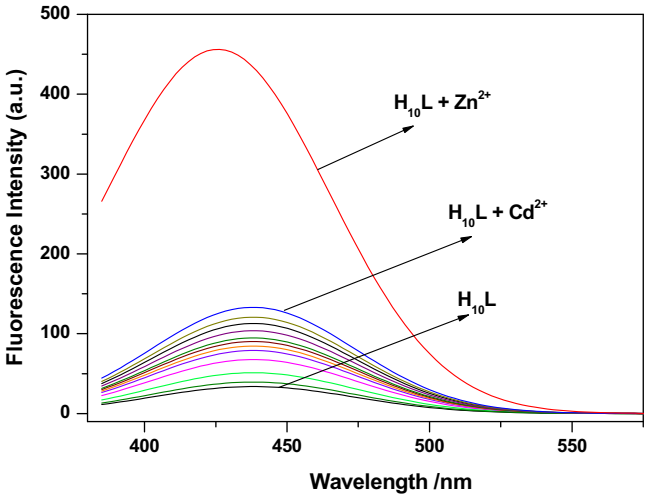

Fig. 2. Change in fluorescence emission spectrum of $\mathbf{H_{10}L}$ (5 μM) in absence (free ligand) and presence of 45 μM concentration of different metal ions at room temperature. Excitation was done at λ_{exc} = 360 nm.

concentration of Fe^{3+} (0–40 μM). It was seen that the absorption peak at 292 nm disappeared and a new absorption peak at 320 nm appeared with gradual addition of Fe^{3+} ion (Fig. 1). Here in presence of Fe^{3+}, an isomerization happened to $\mathbf{H_{10}L}$ due to intramolecular charge transfer (ICT) from O—H and N=CH which leads to imine bond breaking. Thus the conjugation of $\mathbf{H_{10}L}$ was shortened which leads to a drastic color change from colorless to deep yellow in $\mathbf{H_{10}L}$ in presence of Fe^{3+} [49,50].

3.2. Fluorescence studies

Fig. 2 demonstrates the change in fluorescence spectrum of $\mathbf{H_{10}L}$ (~5 μM) in presence of different metal ions like alkali (Na^+, K^+), alkaline earth (Ca^{2+}, Mg^{2+}, Sr^{2+}) and transition metal ions (Cd^{2+}, Ni^{2+}, Co^{2+}, Cu^{2+}, Zn^{2+} and Fe^{3+}) in DMF at room temperature. The fluorescence emission spectrum of $\mathbf{H_{10}L}$ appears a weak, single fluorescence band at 425 nm upon excitation at 360 nm. As soon as Zn^{2+} (45 μM) were added at room temperature, fluorescence emission maxima give red-shift at 435 nm with large increased in fluorescence emission intensity (Fig. 2) and drastic color change occurred from colorless to light brown which can be easily detected with naked eye. However, in presence of other different metal ions

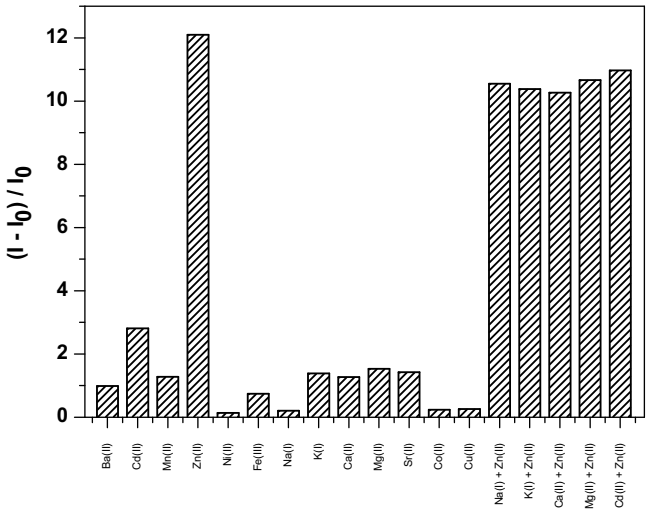

Fig. 3. Fluorescence intensity profile changes of $\mathbf{H_{10}L}$ (5 μM) in absence (free ligand) and presence of 45 μM concentration of various metal ions at room temperature. Fluorescence intensity changes that occur upon subsequent addition of Zn^{2+} ion (45 μM) in presence of different metal ions were also reported. Excitation was done at λ_{exc} = 360 nm.

like Na^+, K^+, Ca^{2+}, Mg^{2+}, Sr^{2+}, Cd^{2+}, Ni^{2+}, Co^{2+} and Fe^{3+}, $\mathbf{H_{10}L}$ showed either no change in fluorescence peak position or a very negligible amount of changes occurs in fluorescence intensity in presence of Cd^{2+} (Fig. 2). This chemosensor was used as a naked eye fluorescent "turn on" detector of Zn^{2+} ion. This clearly indicates that $\mathbf{H_{10}L}$ shows selective estimation for Zn^{2+}, indicating a Zn^{2+} selective OFF-ON fluorescent signalling behavior. However, in presence of Cu^{2+}, it also exhibits quenching of fluorescence emission intensity without any interference of other metal ions present in the solution. Fluorescence intensity profile changes of $\mathbf{H_{10}L}$ in presence of different metal ions were shown in the histogram (Fig. 3) which clearly indicates high selectivity of Zn^{2+}. The increase in fluorescence intensity can be attributed due to the formation of $H_{10}L$-Zn^{2+} complex that inhibits the C=N isomerisation. The binding of metal ion by the C=N group would stop the isomerization of C=N double bond, and a pronounced fluorescence enhancement could be achieved. The appeal of C=N based fluorescent chemosensors is the large fluorescence enhancement induced by metal ion chelation [51]. The sensitivity and selectivity of Zn^{2+} with $\mathbf{H_{10}L}$ was examined with gradual addition of Zn^{2+} concentration (saturated at ~70 μM) as shown in Fig. 4. The fluorescence emission intensity increases remarkably in addition of Zn^{2+} concentration with a red-shift of emission band from 425 nm to 435 nm, which can be explain due to prevention of isomerization by metal ions binding. The enhancement of fluorescence intensity was attributed to the introduction of Zn^{2+} and consequently occurrence of the strong complexation with $\mathbf{H_{10}L}$ via O—H and N heteroatoms. This coordination can enhance the planarity and rigidity which can also decrease nonradiative decay of the excited state and increased radiative decay which may be explained due to photoinduced electron transfer (PET) process between $\mathbf{H_{10}L}$ and Zn^{2+} [52–55]. The fluorescence quantum yields were also calculated both in free ligand as well as in presence of Zn^{2+}. Here, the fluorescence quantum yield was increased drastically from 2.4×10^{-3} for $\mathbf{H_{10}L}$ compared to 8.6×10^{-1} for $H_{10}L$-Zn^{2+} complex.

Further, tolerance of fluorescence intensity due to Zn^{2+} (45 μM) in presence of 50 times an excess of other metal ions like Na^+, K^+, Cd^{2+}, Ca^{2+}, Mg^{2+}, Sr^{2+}, Ni^{2+}, Ba^{2+}, Co^{2+}, Cu^{2+} and Fe^{3+} has been successfully verified as shown in Fig. 3, with no significance changes on the fluorescence intensities rather the fluorescence intensity quenched in presence of Cu^{2+}, Co^{2+} and Ni^{2+} due to unoccupied

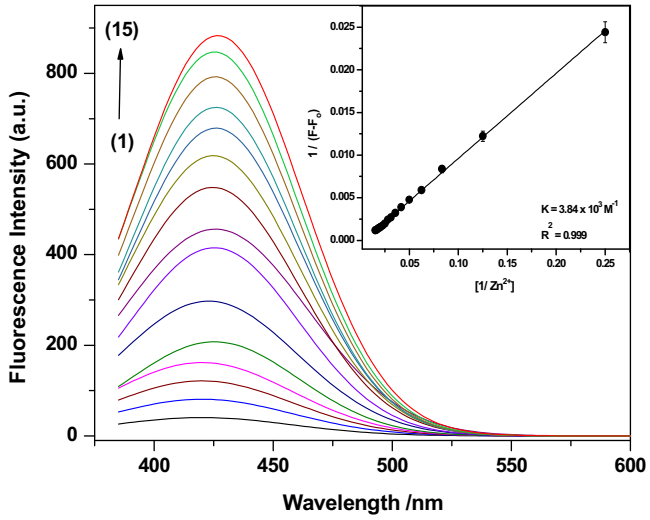

Fig. 4. Variation of fluorescence intensity of $\mathbf{H_{10}L}$ (5 μM) against concentration of Zn^{2+} ion. The concentrations of Zn^{2+} ion (μM) are: 0.0 (1), 5.0 (2), 10.0 (3), 15.0 (4), 20.0 (5), 25.0 (6), 30.0 (7), 35.0 (8), 40.0 (9), 45.0 (10), 50.0 (11), 55.0 (12), 60.0 (13), 65.0 (14) and 70.0 (15). Inset shows the double reciprocal plot for 1:1 complex formation.

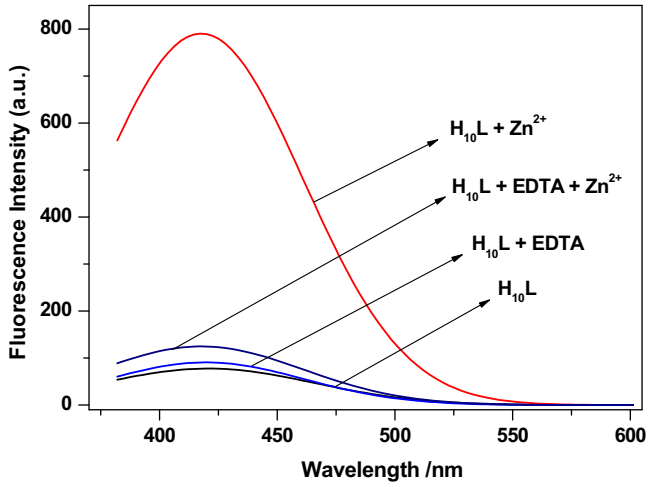

Fig. 5. Fluorescence emission spectra of $\mathbf{H_{10}L}$ (5 μM) in presence of Zn^{2+} ion (60 μM) or EDTA (35 μM) in DMF at room temperature. Excitation was done at λ_{exc} = 360 nm.

molecular d-orbital [56]. Here, in case of Cu^{2+}, Co^{2+} and Ni^{2+}, the fluorescence emission intensity of the probe is highly quenched which may be due to strong binding nature of metal ions with $\mathbf{H_{10}L}$. So, all competitive metal ions had no obvious interference with the detection of Zn^{2+}, which also indicates that $H_{10}L$-Zn^{2+} system was hardly affected by these coexistent metal ions. Thus, $\mathbf{H_{10}L}$ can be used as selective fluorescent chemosensor for Zn^{2+} determination in presence of other competing metal ions.

Furthermore, the reversibility nature of $\mathbf{H_{10}L}$ was studied using a suitable coordinating ligand. Here, we have selected EDTA as a ligand of choice as it is available in abundance and relatively low cost. Fluorescence emission of the complex probe ($H_{10}L$-Zn^{2+}) was monitored with addition of EDTA (~35 μM). The fluorescence emission intensity of the complex probe returned to lower level for $\mathbf{H_{10}L}$ indicate regeneration of free $\mathbf{H_{10}L}$ which corresponds to the fluorescence emission intensity of $\mathbf{H_{10}L}$ (Fig. 5). This regeneration of the free ligand with addition of EDTA was also monitored with the evolution of time. A similar type of reversibility nature for fluorescent sensor has already been reported earlier [57,58]. This may be due to the lack of affinity of EDTA with $\mathbf{H_{10}L}$ as well as its ability

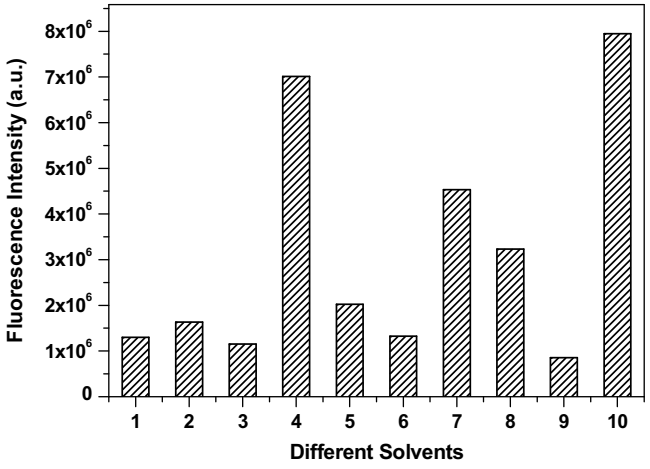

Fig. 6. Fluorescence intensity changes of $\mathbf{H_{10}L}$ (5 μM) in presence of Zn^{2+} ion (60 μM) in different solvents: 1–methanol; 2–ethanol; 3–DMF; 4–THF; 5–1,4–dioxane; 6–ACN; 7–ethylacetate; 8–chloroform; 9–DMSO; 10–toluene at room temperature, respectively. Excitation was done at λ_{exc} = 360 nm.

to form a preferential complex with Zn^{2+} ions. Thus using EDTA, free $\mathbf{H_{10}L}$ was regenerated from $H_{10}L$-Zn^{2+} which can be reused for further Zn^{2+} sensing.

The possibility of using fluorescence probe for determining Zn^{2+} in various homogenous solvents like dimethylsulfoxide (DMSO), N,N dimethylformamide (DMF), methanol, ethanol, ethylacetate, tetrahydrofuran (THF), acetonitrile (ACN), toluene, chloroform and 1,4-dioxane were investigated. Here, the fluorescence intensity enhanced largely in addition of Zn^{2+} to certain solvents like THF, ethylacetate and chloroform (Fig. 6). But there is no significant increase in other solvents. We also knew that THF, ethylacetate and chloroform are hard to be coordinated for the lack of easy-coordinated atom which indicates that no solvent molecule contributes to the coordination. However, this experimental data may be due to inherent complicated properties of the solvent based on their different polarity.

For determination of stoichiometry between $\mathbf{H_{10}L}$ and Zn^{2+}, Job's plot analyses were used. The method is that keeping total concentration of $\mathbf{H_{10}L}$ and Zn^{2+} at 50.0 μM and changing the molar ratio of Zn^{2+} from 0.1 to 1.0. From Fig. 7(a) when molar fraction of Zn^{2+} was 0.5, the fluorescence emission maxima at 435 nm got to maximum, indicating that forming a 1:1 complex between $\mathbf{H_{10}L}$ and Zn^{2+}. Again, the stoichiometric ratio and apparent binding constant of $\mathbf{H_{10}L}$ with Zn^{2+} was determined using Benesi-Hildebrand (BH) relation as fellow [59].

$$\frac{1}{F - F_0} = \frac{1}{F_\alpha - F_0} + \frac{1}{K(F_\alpha - F_0)} \times \frac{1}{[Zn^{2+}]} \quad (2)$$

where, F_0 and F are the fluorescence intensities in the absence and presence of Zn^{2+} respectively. $F\alpha$ is the fluorescence intensity in presence of excess amount of Zn^{2+}. Therefore, for 1:1 complex formation, the double reciprocal plot of $1/(F\text{-}F_0)$ against $1/[Zn^{2+}]$ should give a straight line; from the slope and intercept of which, the equilibrium constant (K) can be calculated. From this plot, we have confirmed 1:1 stoichiometry between $\mathbf{H_{10}L}$ and Zn^{2+} with association constant of $3.8 \times 10^3\ M^{-1}$ (inset of Fig. 4). Moreover, this further corroborated 1:1 complex formation based on Job's plot analyses. Similarly, the association constant between $\mathbf{H_{10}L}$ and Fe^{3+} was also calculated and found to be $1.2 \times 10^4\ M^{-1}$.

We also determine the nature of binding ratio of Zn^{2+} ions to $\mathbf{H_{10}L}$ using other form of BH equation as below:

$$log\frac{I - I_0}{I_{max} - I} = n\log\left[Zn^{2+}\right] - \log K_d \quad (3)$$

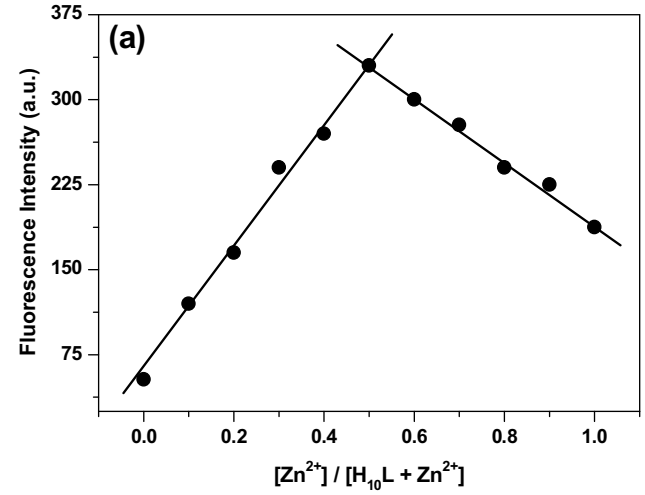

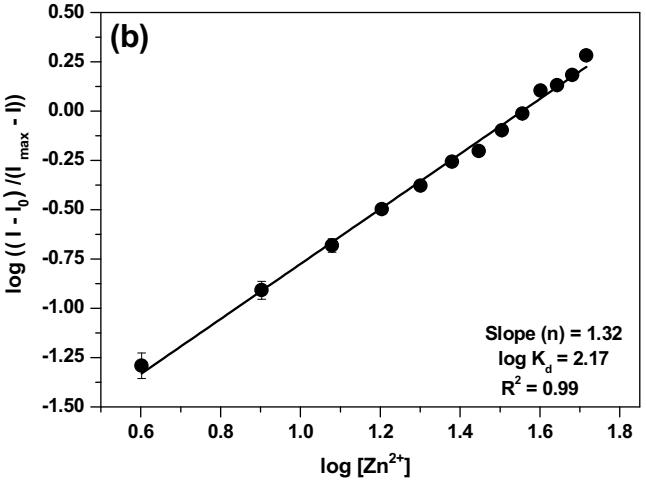

Fig. 7. (a) Job's plot of $\mathbf{H_{10}L}$ (5 μM) with Zn^{2+} ion in DMF at room temperature. (b) Plot of log $((I\text{-}I_o)/(I_{max}\text{-}I))$ versus log $[Zn^{2+}]$ for titration of Zn^{2+} with $\mathbf{H_{10}L}$ in DMF giving slope 1.32 indicates 1:1 complex formation.

where, I_0 and I are the fluorescence intensities in the absence and presence of Zn^{2+} respectively. I_{max} is the fluorescence intensity in presence of excess amount of Zn^{2+}. From the plot of log $((I\text{-}I_o)/(I_{max}\text{-}I))$ versus log $[Zn^{2+}]$ in Eq. (3), the slope and intercept were obtained giving the slope value, n = 1.32 indicating the binding ratio of Zn^{2+} ions to $\mathbf{H_{10}L}$ as 1:1 and log K_d was found out to be 2.17 (Fig. 7(b)).

The emission intensity of $\mathbf{H_{10}L}$ was linearly proportional to Zn^{2+} ion concentration. This linear dependence of Zn^{2+} ion concentration suggests that $\mathbf{H_{10}L}$ could be utilized for the quantitative estimation of Zn^{2+}. The detection limit was calculated using 3*S/M [60] where S is the standard deviation of a blank signal and M is the slope of the regression line. The detection limit was found to be in order of 10×10^{-6} M. Hence, $\mathbf{H_{10}L}$ shows selective estimation for Zn^{2+} and "turn-on" fluorescent sensor in presence of Zn^{2+} ion. Similarly, the detection limit for Fe^{3+} ion was also calculated and found to be 2.6×10^{-6} M. A comparison of the analytical performances of the present work with available literature report for determination of Zn^{2+} and Fe^{3+} ions analysis in terms of binding constant and detection limits are summarized in Table 1. As can be seen from Table 1, most of these methods have different performance values for good sensitivity. However, in comparison with other methods, this sensor has comparatively more sensitivity and lower detection limit value compared to other fluorescent sensors [61–65].

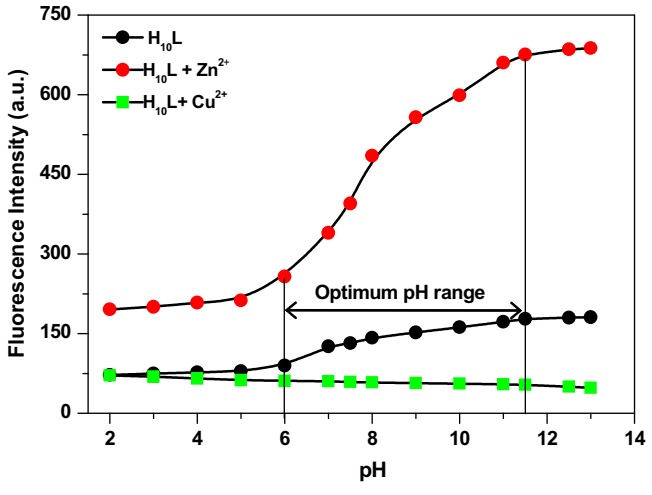

Fig. 8. Effect of pH on the fluorescence intensity of $\mathbf{H_{10}L}$ (5 μM) in absence (●) and presence (●) of Zn^{2+} ion and (■) of Cu^{2+} ion.

Since, many fluorescent probe are sensitive to pH, we also studied sensitivity to pH in presence and absence of Zn^{2+} and Cu^{2+} (Fig. 8). Over a wide range of pH, there was no obvious change in fluorescence intensity of free ligand alone which indicates insensitivity to pH. However, in presence of Zn^{2+}, $\mathbf{H_{10}L}$ has a strong pH dependent in the wide pH range from pH 6.0 to pH 11.5 with satisfactory Zn^{2+} sensing abilities. Thus, $\mathbf{H_{10}L}$ indicates a good fluorescence sensing ability to Zn^{2+} over a wide range of pH = 6.0-11.5. However, on addition of Cu^{2+}, quenching behaviour was observed in the wide pH range from pH 4.0 to pH 11.5. These results also clearly indicate that $\mathbf{H_{10}L}$ can be employed as a selective fluorescent probe to recognize and distinguish Zn^{2+} and Cu^{2+} in presence of other different metal ions. Moreover, $\mathbf{H_{10}L}$ forms stable complex with Zn^{2+} and Cu^{2+} in this wide pH range.

Metal-ligand complexes have been studied showing both the affect on fluorescence emission wavelength and intensity of the ligand through metal coordination. Herein, the fluorescence behaviours of $\mathbf{H_{10}L}$ and complexes with different substituent of Zn^{2+} were studied in the solution phase at room temperature. Here, the emission spectra of complexes are very similar with $\mathbf{H_{10}L}$ except for the fluorescence intensity and peak position, indicating that the fluorescence of complexes is L-based emission. Meanwhile, the fluorescence emission for complexes were slightly red-shifted compared to free ligand which are considered to mainly arise from the coordination of Zn^{2+} centres to $\mathbf{H_{10}L}$. The incorporation of Zn^{2+} effectively increases the conformational rigidity of the ligand and enhanced fluorescence intensities of all five complexes [66]. Moreover, from Fig. 9, the different in fluorescence intensities of the complexes with different substituent's like SO_4, Cl, NO_3, CO_3 and CH_3COO, can be explain due to bigger conformational rigidity for a 3D supramolecular network, as well as hydrogen bonds and π. . ..π packing interactions [67].

In order to evaluate the application feasibility to determine Zn^{2+} ion in real water samples, several water samples from different water sources were selected including tap water, ground water, river water, pond water, drinking water and deionised water. The changes in fluorescence emission intensity were measured after addition of 50% of the water samples to DMF solution of the probe (Fig. 10). Here, the fluorescence intensity of the probe upon addition of 50% tap and ground water indicate significant increased compare to other water samples, which indicates the content of Zn^{2+} ion in tap and ground water is comparatively very high. However, in case of river and pond water, the fluorescence intensity is weak compare to tap and ground water which indicate low content of the Zn^{2+} or

Table 1
Comparison between proposed sensor and previously reported literature values for Zn^{2+} and Fe^{3+} ions sensors.

Systems	Detection Limit		Binding Constant		Refs.	Methods
	Zn^{2+}	Fe^{3+} (M)	Zn^{2+} (M^{-1})	Fe^{3+} (M^{-1})		
N,N′,N″-tris(salicylidene)(2-aminoethyl) amine	1.1 μM		$\log K_a = 4.52$		[61]	Absorbance
3-(1H-imidazo[4,5-*f*][1,10]phenanthrolin-2-yl) phenylboronic acid	6.74×10^{-7} M		1.50×10^5		[62]	Fluorescence
Julolidine based Schiff base	1.59 μM	0.22×10^{-6}	2.9×10^4	1.2×10^4	[63]	Fluorescence/ Absorbance
Julolidine based Schiff base	15.6 μM	6.8×10^{-6}	1.0×10^8	3.3×10^4	[64]	Absorbance
(*R*)-2-[3-(4-(diethylamino)salicylaldimine]- phenyglycinol	4.98×10^{-7} M		$\log K_a = 12.2$		[65]	Fluorescence
(*E*)-2-(((8-hydroxyquinolin-2-yl)methylene)amino)-6H-benzo[c]chromen-6-one ($\mathbf{H_{10}L}$)	10×10^{-6} M	2.6×10^{-6}	3.8×10^3 ($\log K_d = 2.17$)	1.2×10^4 ($\log K_d = 2.9$)	This Work	Fluorescence

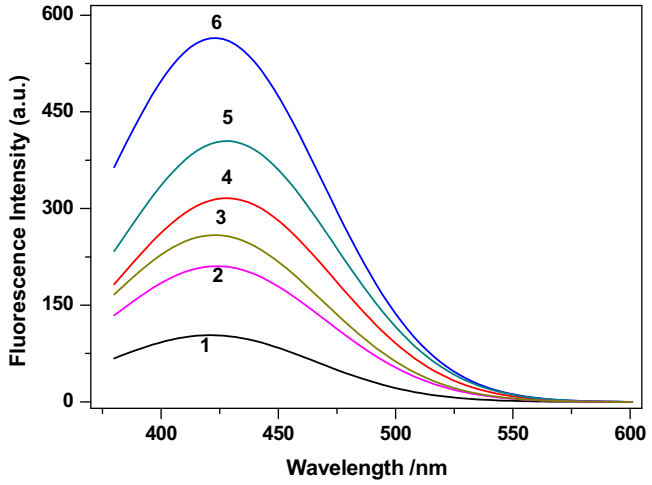

Fig. 9. Fluorescence emission spectra of $\mathbf{H_{10}L}$ (5 μM) in complexes with different substituents; ligand (**1**-free ion) and complexes with Zn^{2+} ion (**2**-nitrate, **3**-carbonate, **4**-sulphate, **5**-chloride and **6**-acetate) in the solution phase at room temperature, respectively.

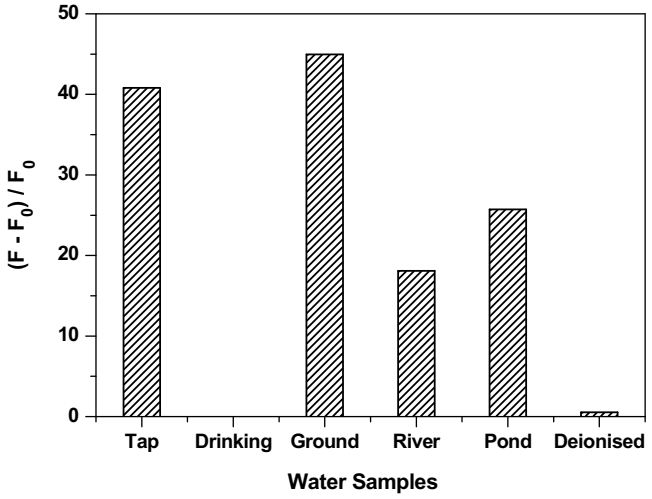

Fig. 10. Fluorescence intensity of $\mathbf{H_{10}L}$ (5 μM) with addition of 50% (%, v/v) water samples in DMF at room temperature.

due to the presence of different interfering metal ions. For drinking and deionised water, there is almost negligible enhancement of fluorescence intensity which suggests that the amount of Zn^{2+} ion in these two samples is very low.

3.3. ^1H NMR titration and mass analysis

In order to understand the interaction and binding nature of $\mathbf{H_{10}L}$ towards Zn^{2+} ion, ^1H NMR titration experiments were carried out before and after addition of different concentrations of Zn^{2+} ion in DMSO-d_6 solvent at room temperature. As shown in Fig. 11, the hydroxyl proton of $\mathbf{H_{10}L}$ obtained at around 9.10 ppm in the free ligand has experienced a remarkable downfield shift towards 9.40 ppm upon addition of Zn^{2+} ion. On the other hand, the aromatic protons signal at 8.79, 8.44, 8.1, 7.87, 7.65 ppm were shifted upfield to 8.54, 8.06, 7.76, 7.53, 7.38 ppm while the other signals at 8.6, 7.79, 7.68, 7.61 ppm were shifted downfield to 8.63, 8.73, 8.33, 8.23 ppm in presence of Zn^{2+} ion, respectively. These spectra exhibited the binding nature of $\mathbf{H_{10}L}$ with Zn^{2+} ion in 1:1 stiochiometric ratio [68,69]. Moreover, these overall changes in the chemical shifts of the proton in presence of Zn^{2+} ions suggested that the binding of $\mathbf{H_{10}L}$ to Zn^{2+} forms a rigid system by a strong complexation with $\mathbf{H_{10}L}$ via O—H and N heteroatoms.

To better understand the binding nature of $\mathbf{H_{10}L}$ with Zn^{2+} ion, ESI-mass spectra of $\mathbf{H_{10}L}$ and its complex ($H_{10}L$-Zn^{2+}) were recorded and shown in Fig. 12. The observed *m*/*z* peak for $\mathbf{H_{10}L}$ was obtained at 366.10. However, in presence of Zn^{2+} ion, the *m*/*z* peak was found to be at 425.10 which correspond to $[H_{10}L+Zn^{2+}+Acetate]^+$ (calculated: 425.02). So, these mass spectra also confirmed the binding nature of $\mathbf{H_{10}L}$ to Zn^{2+} as 1:1 stoichiometry [70–72].

3.4. Time-resolved fluorescence measurements

Fluorescence decay time of $\mathbf{H_{10}L}$ is detected by nanosecond time-correlated single photon counting technique using 360 nm LED source and monitoring the emission at 425 nm. The fluorescence decay curves were analyzed by non-linear least-square iterative convolution method using Eq. (4) based on Lavenberg-Marquardt [73] chi-sqare (χ^2) minimization algorithm (Eq. (5))

$$F(t) = \sum_i \alpha_i \exp(-t/\tau_i) \quad (4)$$

α_i is the associated pre-exponential factor corresponding to the decay time τ_i.

$$\chi^2 = \frac{\sum_{i=1}^{N} [y_i - f(x_i)]^2}{N - P} \quad (5)$$

N is the number of data points and P is the number of free parameters in the fitting function. The reliability of fitting was checked by numerical value of reduced chi-sqare (χ^2) and also Durbin-Watson (DW) parameter.

Here, the fluorescence decay need three exponential function both for free ligand as well as the complex probe ($H_{10}L$-Zn^{2+}) to

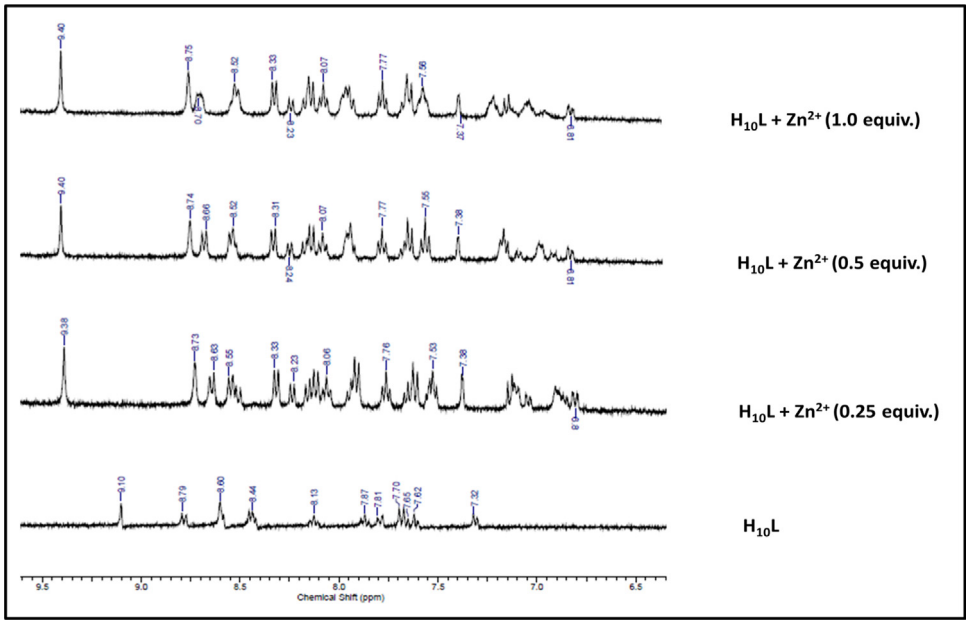

Fig. 11. ^{1}H NMR titration plot of $\mathbf{H_{10}L}$ with Zn^{2+} ion in DMSO-d_6 solvent.

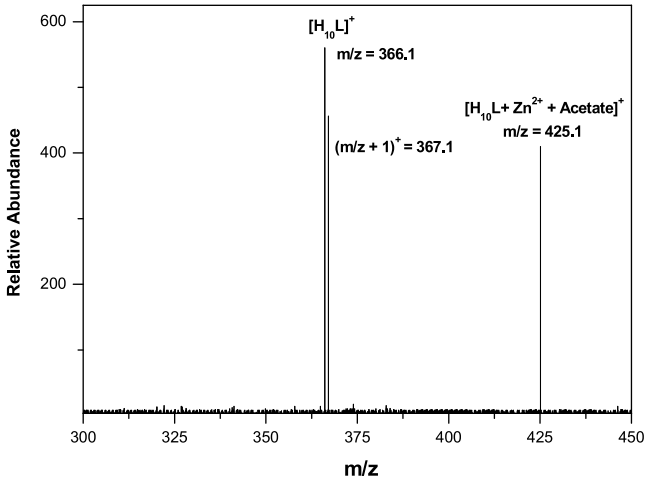

Fig. 12. ESI–MS spectra of $\mathbf{H_{10}L}$ and its complex ($H_{10}L$-Zn^{2+}).

reproduce the experimental data points with acceptable statistical parameters like reduced chi-square (χ^2) values and Durbin-Watson parameter as demonstrated by visual inspection of the distribution of weighted residuals with time (Fig. 13). The multiexponential fluorescence decay parameters for $\mathbf{H_{10}L}$: $\tau_1 = 0.15$ ns (0.45), $\tau_2 = 2.5$ ns (0.40) and $\tau_3 = 8.6$ ns (0.15) and for $H_{10}L$-Zn^{2+}: $\tau_1 = 0.21$ ns (0.40), $\tau_2 = 2.9$ ns (0.47) and $\tau_3 = 23.2$ ns (0.13), respectively. The multiexponential fluorescence decay may appear due to several reasons and sometimes, it is very difficult to give mechanistic assignment to individual components. However, it is seen that the amplitude of the short nanosecond component is much larger compared to long nanosecond component. This complex nature of the fluorescence decay parameters is a reflection of the flexibility of the molecules [74]. Instead of giving too much importance to individual decay components, we calculate the average decay time of $\mathbf{H_{10}L}$ both in free ligand and complex probe ($H_{10}L$-Zn^{2+}) using Eq. (6) to discuss the fluorescence decay behavior.

$$< \tau >= \sum_i \alpha_i \times \tau_i \qquad (6)$$

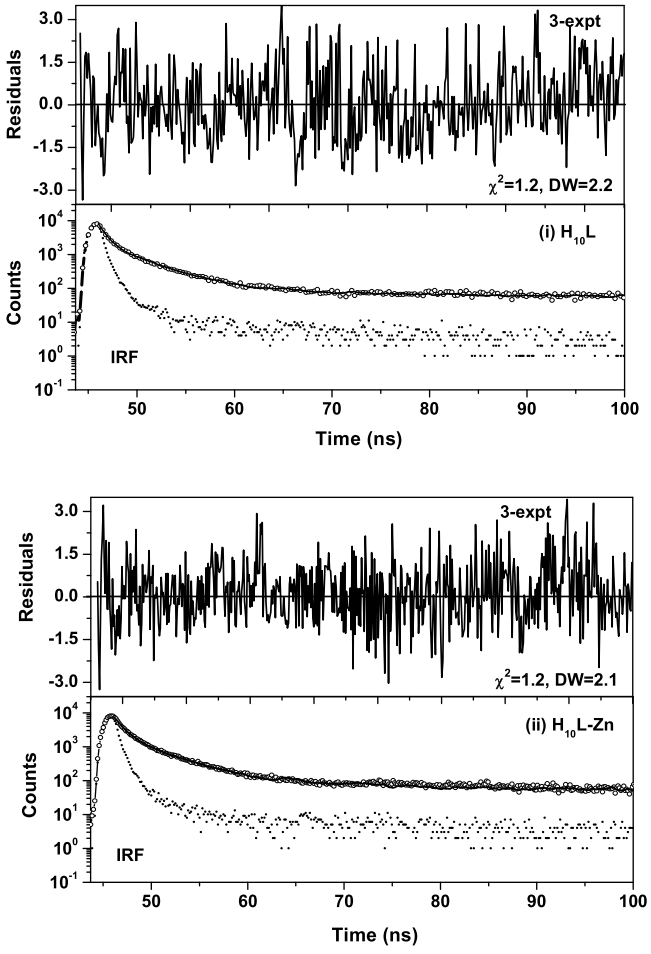

Fig. 13. Time-resolved fluorescence decay profile of $\mathbf{H_{10}L}$ in absence (free ligand) and presence of Zn^{2+}, respectively. IRF indicates instrument response function. The upper panels show the distribution of weighted residuals for three exponential fitting along with reduced chi-square (χ^2) and Durbin-Watson (DW) parameters in each case.

INPUT		OUTPUT
IN1	IN2	OUT
Zn^{2+}	Cu^{2+}	Emission at 435 nm
0	0	0
0	1	0
1	0	1
1	1	0

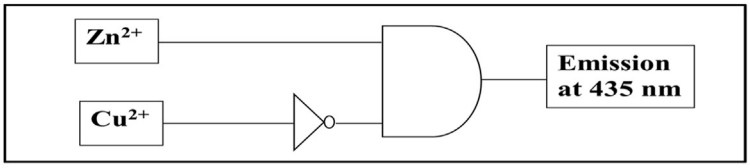

(a) Zn^{2+} and Cu^{2+}

INPUT		OUTPUT
IN1	IN2	OUT
Zn^{2+}	EDTA	Emission at 435 nm
0	0	0
0	1	0
1	0	1
1	1	0
INPUT		OUTPUT
IN1	IN2	OUT
Cu^{2+}	EDTA	Emission at 435 nm
0	0	1
0	1	1
1	0	0
1	1	1

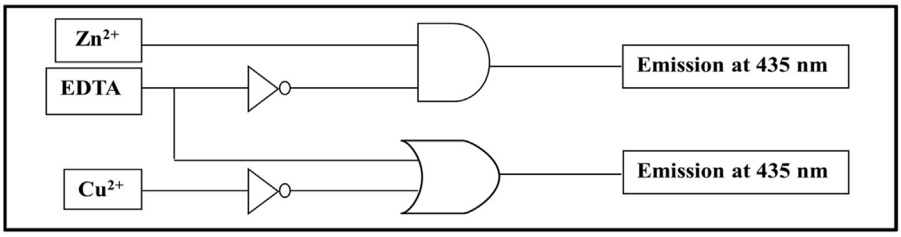

(b) Zn^{2+} with EDTA and EDTA with Cu^{2+}

Fig. 14. Truth table and the monomolecular circuit based on (a) Zn^{2+} and Cu^{2+} and (b) Zn^{2+} with EDTA and EDTA with Cu^{2+}.

The calculated average fluorescence decay values are 2.35 ns and 4.46 ns for free ligand and the complex probe ($H_{10}L$-Zn^{2+}), respectively. It is interesting to note that the average fluorescence decay time in ($H_{10}L$-Zn^{2+}) is about two times larger than the corresponding values in $\mathbf{H_{10}L}$. Here, we found that the fluorescence decay time was affected by turn-on sensor in presence of Zn^{2+}.

3.5. Application of logic function

The fluorescence emission behavior of $\mathbf{H_{10}L}$ can be utilised to study as a binary logic function with dual stimulating inputs as Zn^{2+} (IN1) and Cu^{2+} (IN2) and emission as output. With coordination of $\mathbf{H_{10}L}$ with Zn^{2+} (IN1) a new fluorescence emission band appears at 425 nm. Upon gradual addition of Cu^{2+} (IN2), the emission intensity of the band at 425 nm gets quenched. This can be explaining due to preference in binding of $\mathbf{H_{10}L}$ with Cu^{2+} even in presence of Zn^{2+}. Herein, the coordination complex of $H_{10}L$-Zn^{2+} is replaced with Cu^{2+} due to greater abilities of binding with Cu^{2+} rather than Zn^{2+}. The threshold value of fluorescence emission intensity is considered to be 300. OUT = 0 when intensity is less than 300; OUT = 1 when intensity is higher than 300. Now OUT = 1 only when Zn^{2+} is present alone. Actually it represents an AND gate with an inverter [75] in one of its input. Thus the emission change at 425 nm with Zn^{2+} as well as Cu^{2+} (with an invertor) as inputs can be interpreted as a monomolecular circuit showing an INHIBIT logic function [18] (Fig. 14 (a)).

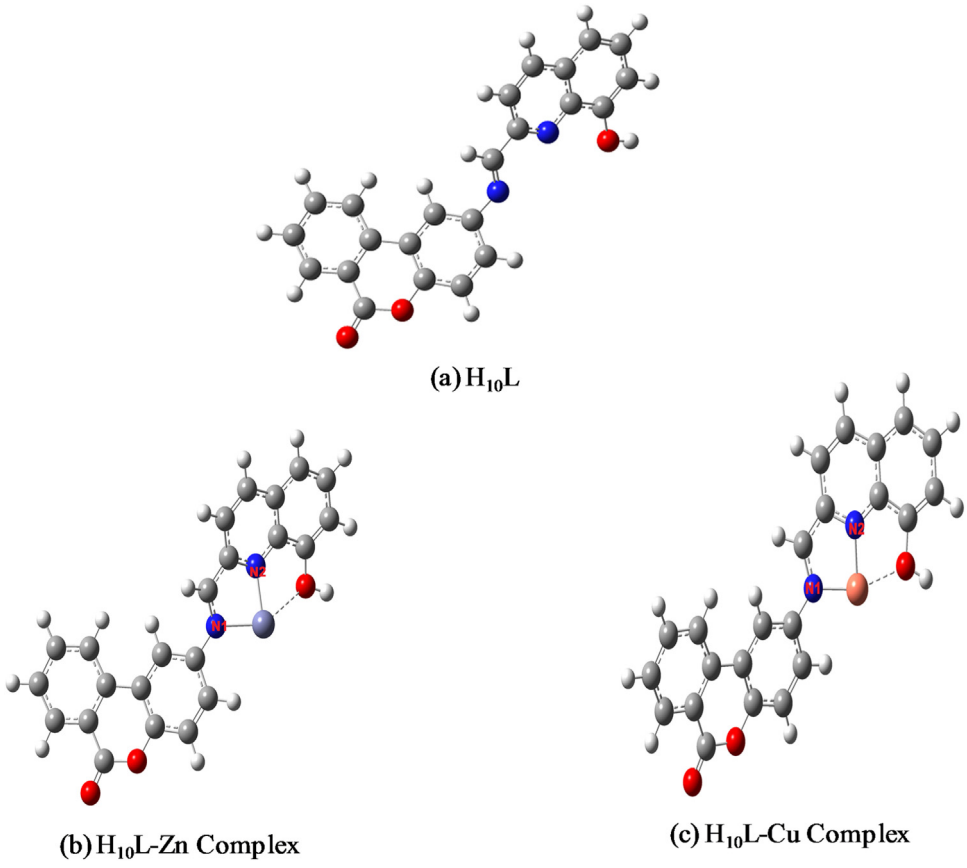

Fig. 15. DFT optimized structures of $\mathbf{H_{10}L}$, Zn-complex and Cu-complex evaluated at B3LYP level along with 6–31G** basis set.

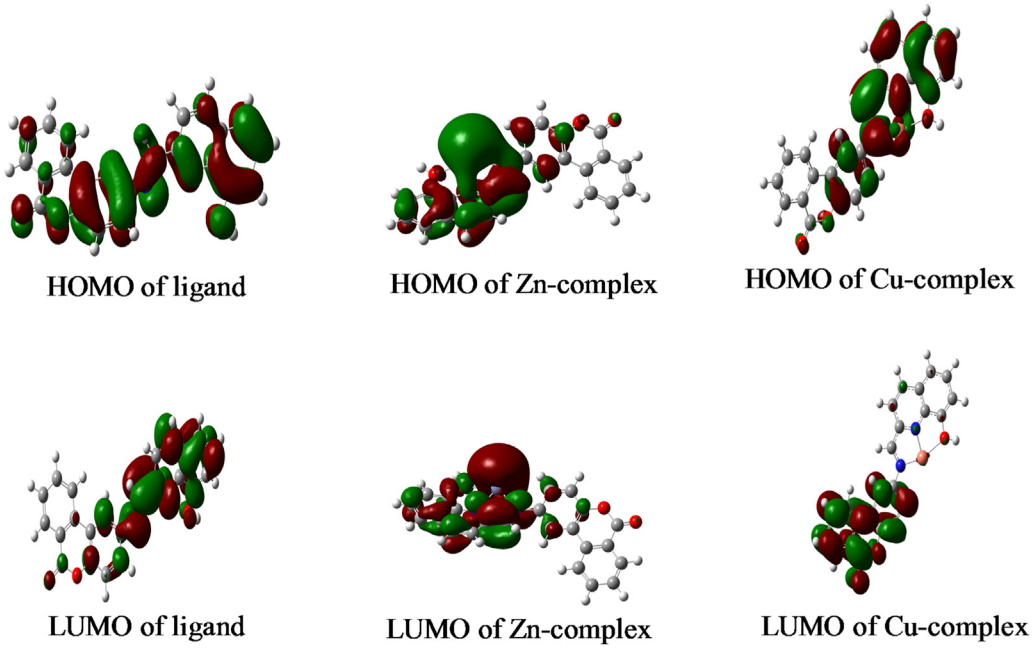

Fig. 16. DFT evaluated 3D isosurface HOMO and LUMO diagrams of $\mathbf{H_{10}L}$, Zn-complex and Cu-complex, respectively.

The regeneration of the free ligand was monitored with addition of EDTA as a good chelating agent. Here, the fluorescence emission intensity of the complex probe ($H_{10}L$-Zn^{2+}) returned to lower level for $\mathbf{H_{10}L}$ in presence of EDTA (~35 μM) which corresponds to the fluorescence emission intensity of the free ligand. The decrease of fluorescence emission intensity and the emission band at 425 nm is almost disappeared indicating regeneration of free ligand. However in the absence of Zn^{2+}, EDTA does not have any effect on the emission intensity of $\mathbf{H_{10}L}$ (Fig. 5). Thus, with two chemical inputs as Zn^{2+} (IN1) and EDTA (IN2) and the emission as output, the

molecular logic function was studied. The threshold value of fluorescence emission intensity is considered to be 300. OUT = 0 when intensity is less than 300; OUT = 1 when intensity is higher than 300. Here, $\mathbf{H_{10}L}$ functions as an AND gate with an inverter in the EDTA input by monitoring the emission output. This function can be interpreted as a monomolecular circuit showing an INHIBIT logic function (Fig. 14(b)). As we know, upon addition of Cu^{2+}, the fluorescence emission intensity band of $\mathbf{H_{10}L}$ at 425 nm gets quenched. However, with addition of EDTA as chelating agent to this complex ($H_{10}L$-Cu^{2+}), a pronounced fluorescence enhancement is observed which may be due to complex formation of EDTA with Cu^{2+} making the ligand free. So, in presence of EDTA to this complex, the fluorescence emission intensity is high compare only when Cu^{2+} is present alone. Thus, this behavior represents an OR gate with an inverter in one of its input which is also called an IMPLICATION logic gate [76] (Fig. 14 (b)).

3.6. Theoretical calculation

Density functional theory (DFT) calculation is performed to investigate the electronic structure of ligand and its metal complexes. Full geometry optimization of ligand and its metal complexes has been carried out without imposing any constrain using Becke's three parameter hybrid exchange functional (B3) and the Lee-Yang-Parr correlation functional (LYP) (B3LYP) along with 6–31G** basis set. In order to confirm the stability of ligand and its metal complexes, we performed vibrational frequency calculations at the same level of theory. No imaginary frequency of the optimized geometries of ligand and its metal complexes suggest that the optimized geometry represents stable structures (local minima) in the potential energy surfaces which are shown in Fig. 15. It is seen from Fig. 15 that both zinc and copper metal centre are tri coordinated to the ligand through imine and quinoline nitrogen atoms and one OH group of ligand. It is noted from DFT generated data that selected bond lengths (Å) and bond angles (°) for both Zn-complex and Cu-complex has been evaluated at B3LYP level. In Zn-complex, the bond length (Å) of Zn—N(1), Zn—N(2) and Zn—O are 2.016 Å, 1.971 Å and 2.635 Å, respectively. However, in case of Cu-complex, the bond length (Å) of Cu—N(1), Cu—N(2) and Cu—O are 1.908 Å, 1.905 Å and 2.295 Å, respectively. Here, metal-OH bond lengths in both complexes are longer than the other bond lengths. Moreover, the bond angles N(1)—Zn—N(2) and N(1)—Cu—N(2) are found to be 82.56° and 83.73°, respectively, around the metal atom. DFT evaluated bond angles deviate substantially from planer geometry.

Lowest unoccupied molecular orbital (LUMO) and highest occupied molecular orbital (HOMO) energies are calculated to be −2.19 eV and −5.86 eV for ligand. In Zn-complex energies of LUMO and HOMO are −2.41 eV and −4.04 eV respectively and also in Cu-complex respective LUMO and HOMO energies are −2.21 eV and −4.22 eV. The corresponding energy difference ΔE (E_{LUMO}-E_{HOMO}) of the ligand, zinc and copper complexes are found to be 3.67, 1.63 and 2.01 eV, respectively. From the 3D isosurface HOMO and LUMO diagram (Fig. 16) of the Zn-complex, it is observed that the electron density of this complex is located on both zinc centre and ligand moiety but in case of the Cu-complex the electron density is mainly ligand character in LUMO whereas in HOMO the electron density is located on both ligand and copper metal. We further calculated the chemical hardness ($\eta = \frac{E_{LUMO}-E_{HOMO}}{2}$) [77] values for the ligand as well as the Zn-complex and Cu-complex from their LUMO and HOMO energies. The chemical hardness values of ligand, Zn-complex and Cu-complex are found to be 1.835, 0.815 and 1.005 eV, respectively. Higher hardness value of the ligand reveals higher stability of the ligand than its respective complexes. The Cu-complex found to be more stable than Zn-complex as Cu-complex has higher hardness value than Zn-complex.

4. Conclusions

In this work, we have successfully designed and synthesized a new coumarin based Schiff-base dual chemosensor-(*E*)-2-(((8-hydroxyquinolin-2-yl)methylene)amino)-6H-benzo[c] chromenone ($\mathbf{H_{10}L}$) which has been evaluated as a colorimetric sensor for Fe^{3+} and fluorescence turn-on response for Zn^{2+}. Upon treatment with Fe^{3+} and Zn^{2+}, the absorption intensity as well as the fluorescence emission intensity increases drastically with a distinct color change which provide naked eye detection. However, other common alkali, alkaline earth and transition metal ions failed to induce response or minimal spectral changes. Fluorescence studies on $\mathbf{H_{10}L}$ and $H_{10}L$-Zn^{2+} complex reveal that the quantum yield strongly increases upon coordination. The complex solution of $\mathbf{H_{10}L}$ with Zn^{2+} ion exhibited reversibility with EDTA and regenerate free ligand for further Zn^{2+} sensing. The stoichiometric ratio and association constant were evaluated using Benesi-Hildebrand relation giving 1:1 stoichiometry. This further corroborated 1:1 complex formation based on Job's plot analyses. This chemosensor exhibits a very good fluorescence sensing ability to Zn^{2+} over a wide pH range. This chemosensor can be used as an important application for detection of Zn^{2+} in real water samples. $\mathbf{H_{10}L}$ exhibits an INHIBIT logic gate with Zn^{2+} and EDTA as chemical inputs and the emission as output. Again, an IMPLICATION logic gate is obtained with Cu^{2+} and EDTA as chemical inputs and emission as output mode. Both $\mathbf{H_{10}L}$ and metal-complexes are optimised using density functional theory and vibrational frequency calculations confirm that both are at local minima on the potential energy surfaces. The corresponding energy difference ΔE (E_{LUMO}-E_{HOMO}) of $\mathbf{H_{10}L}$, Zn-complex and Cu-complex are found to be 3.67, 1.63 and 2.01 eV, respectively. The chemical hardness values of ligand, Zn-complex and Cu-complex are found to be 1.835, 0.815 and 1.005 eV, respectively. The Cu-complex is found to be more stable than Zn-complex as Cu-complex has higher hardness value than Zn-complex. Moreover, this work provides a new approach with economically cheap and less complicated synthetic route for selectively and sensitively estimation of these two most abundant and essential traces elements in the human body.

Acknowledgements

Financial support through Start-Up Research Grant (Chemical Sciences) project No. SB/FT/CS-064/2012 from Science and Engineering Research Board (SERB), Government of India were gratefully acknowledged by Dr. T. Sanjoy Singh. The authors are indebted to Dr. S. Mitra and his research scholars for their help in TCSPC measurements. The authors are also highly acknowledged to CIF, IIT Guwahati for providing NMR and Mass spectra.

References

[1] R. Krämer, Fluorescent chemosensors for Cu^{2+} ions: fast, selective, and highly sensitive, Angew. Chem. Int. Ed. 37 (1998) 772–773.
[2] R. Uauy, M. Olivares, M. Gonzalez, Essentiality of copper in humans, Am. J. Clin. Nutr. 67 (1998) 952–959.
[3] A.P. de Silva, H.Q.N. Gunaratne, T. Gunnlaugsson, A.J.M. Huxley, C.P. McCoy, J.T. Rademacher, T.E. Rice, Signaling recognition events with fluorescent sensors and switches, Chem. Rev. 97 (1997) 1515–1566.
[4] A.W. Czarnik, Fluorescent Chemosensors for Ion and Molecule Recognition, 1st ed., A.C.S, Washington, 1992.
[5] Y. Lu, S.M. Berry, T.D. Pfister, Engineering novel metalloproteins: design of metal-binding sites into native protein scaffolds, Chem. Rev. 101 (2001) 3047–3080.
[6] S. Narayanaswamy, T. Govindaraju, Aldazine-based colorimetric sensors for Cu^{2+} and Fe^{3+}, Sens. Actuators B 161 (2012) 304–310.

[7] B.L. Vallee, K.H. Falchuk, The biochemical basis of zinc physiology, Physiol. Rev. 73 (1993) 79–118.
[8] J.J.R.F. de Silva, R.J.P. Williams, The Biological Chemistry of Elements: The Inorganic Chemistry of Life, 2nd ed., Oxford University Press, New York, 2001.
[9] A.I. Bush, W.H. Pettingell, G. Multhaup, M. Paradis, J.P. Vonsattel, J.F. Gusella, K. Beyreuther, C.L. Masters, R.E. Tanzi, Rapid induction of Alzheimer A beta amyloid formation by zinc, Science 265 (1994) 1464–1467.
[10] J.Y. Koh, S.W. Suh, B.J. Gwag, Y.Y. He, C.Y. Hsu, D.W. Choi, The role of zinc in selective neuronal death after transient global cerebral ischemia, Science 272 (1996) 1013–1016.
[11] C.F. Walker, R.E. Black, Zinc and the risk for infectious disease, Annu. Rev. Nutr. 24 (2004) 255–275.
[12] S.K. Danuta, R.R. Des, The evolution of iron chelators for the treatment of iron overload disease and cancer, Pharmacol. Rev. 579 (2005) 547–583.
[13] A.P. de silva, H.Q. Nimal Gunarane, C.P. McCoy, A molecular photoionic AND gate based on fluorescent signalling, Nature 364 (1993) 42–44.
[14] K. Szacilowski, Digital information processing in molecular systems, Chem. Rev. 108 (2008) 3481–3548.
[15] (a) A.P. de Silva, N.D. McClenaghan, Molecular-scale logic gates, Chem. Eur. J. 10 (2004) 574–586.
[16] K. Rurack, C. Trieflinger, A. Koval'chuck, J. Daub, An ionically driven molecular implication gate operating in fluorescence mode, Chem. Eur. J. 13 (2007) 8998–9003.
[17] (a) L. Zhao, D. Sui, J. Chai, Y. Wang, S. Jiang, Digital logic circuit based on a single molecular system of salicylidene schiff base, J. Phys. Chem. B. 110 (2006) 24299–24304.
[18] (a) N. Kaur, N. Singh, D. Caims, J.F. Callan, A multifunctional tripodal fluorescent probe: off-On detection of sodium as well as two-input AND molecular logic behavior, Org. Lett. 11 (2009) 2229–2232.
[19] (a) D. Sarkar, A. Pramanik, S. Biswas, P. Karmakar, T.K. Mondol, Al^{3+} selective coumarin based reversible chemosensor: application in living cell imaging and as integrated molecular logic gate, RSC Adv. 4 (2014) 30666–30672.
[20] (a) V.K. Gupta, S. Jain, S. Chandra, Chemical sensor for lanthanum(III) determination using aza-crown as ionophore in poly(vinyl chloride) matrix, Anal. Chim. Acta 486 (2003) 199–207;
(b) V.K. Gupta, S. Chandra, R. Mangla, Dicyclohexano-18-crown-6 as active material in PVC matrix membrane for the fabrication of cadmium selective potentiometric sensor, Electrochim. Acta 47 (2002) 1579–1586;
(c) V.K. Gupta, S. Juin, U. Khurana, A PVC-based pentathia-15-crown4 membrane potentiometric sensor for mercury (II), Electroanalysis 9 (1997) 478–480;
(d) S.K. Srivastava, V.K. Gupta, S. Jain, Determination of lead using a poly(viny1chloride)-based crown ether membrane, Analyst 120 (1995) 495–498;
(e) S.K. Srivastava, V.K. Gupta, M.K. Dwivedi, S. Jain, Caesium PVC-Crown (Dibenzo-24- crown-8) Based Membrane Sensor, Anal. Proc. Incl. Anal. Commun. 32 (1995) 21–23.
[21] (a) R. Gupta, U. Mangla, Determination of uranyl ions using poly(vinyl chloride) based 4-tert-Butylcalix[6] arene membrane sensor, Electroanalysis 11 (1999) 573–576;
(b) B. Gupta, R.A. Sethi, S. Sharma, A. Agarwal, Mercury selective potentiometric sensor based on low rim functionalized thiacalix [4]-arene as a cationic receptor, J. Mol. Liq. 177 (2013) 114–118.
[22] (a) A.K. Jain, V.K. Gupta, L.P. Singh, U. Khurana, Macrocycle based membrane sensors for the determination of cobalt(II) ions, Analyst 122 (1997) 583–586.
[23] (a) V.K. Gupta, A. Nayak, S. Agarwal, B. Singhal, Recent advances on potentiometric membrane sensors for pharmaceutical analysis, Combi. Chem. High Throughput Screening 14 (2011) 284–302.
[24] V.K. Gupta, M.R. Ganjali, P. Norouzi, H. Khani, A. Nayak, S. Agarwal, Electrochemical analysis of some toxic metals by ion–selective electrodes, Crit. Rev. Anal. Chem. 41 (2011) 282–313.
[25] V.K. Gupta, R. Prasad, P. Kumar, R. Mangla, New nickel(II) selective potentiometric sensor based on 5,7,12,14-tetramethyldibenzotetraazaannulene in a poly(vinyl chloride) matrix, Anal Chim. Acta 420 (2000) 19–27.
[26] V.K. Gupta, L.P. Singh, R. Singh, N. Upadhyay, S.P. Kaur, B. Sethi, A novel copper (II) selective sensor based on Dimethyl 4, 4′ (o-phenylene) bis(3-thioallophanate) in PVC matrix, J. Mol. Liq. 174 (2012) 11–16.
[27] V.K. Gupta, A.K. Jain, G. Maheshwari, Aluminum(III) selective potentiometric sensor based on morin in poly(vinyl chloride) matrix, Talanta 72 (2007) 1469–1473.
[28] V.K. Gupta, A.K. Jain, S. Agarwal, G. Maheshwari, An iron(III) ion-selective sensor based on a μ-bis(tridentate) ligand, Talanta 71 (2007) 1964–1968.
[29] A.K. Jain, V.K. Gupta, U. Khurana, L.P. Singh, A new membrane sensor for UO_2^{2+} ions based on 2-hydroxyacetophenoneoxime-thiourea-trioxane resin, Electroanalysis 9 (1997) 857–860.
[30] V.K. Gupta, R.N. Goyal, R.A. Sharma, Anion recognition using newly synthesized hydrogen bonding disubstituted phenylhydrazone-based receptors: poly(vinyl chloride)-based sensor for acetate, Talanta 76 (2008) 859–864.
[31] H. Khania, M.K. Rofoueia, P. Arabb, V.K. Gupta, Z. Vafaeia, Multi-walled carbon nanotubes-ionic liquid-carbon paste electrode as a super selectivity sensor: application to potentiometric monitoring of mercury ion(II), J. Hazard. Mater. 183 (2010) 402–409.
[32] V.K. Gupta, H. Karimi-Maleh, R. Sadegh, Simultaneous determination of hydroxylamine, phenol and sulfite in water and waste water samples using a voltammetric nanosensor, Int. J. Electrochem. Sci. 10 (2015) 303–316.
[33] L. Salmon, P. Thuéry, E. Rivière, M. Ephritikhine, Synthesis structure, and magnetic behavior of a series of trinuclear schiff base complexes of 5f (U^{IV}, Th^{IV}) and 3d (Cu^{II}, Zn^{II}) ions, Inorg. Chem. 45 (2006) 83–93.
[34] D.M. Epstein, S. Choudhary, M.R. Churchill, K.M. Keil, A.V. Eliseev, J.R. Morrow, Chloroform-Soluble schiff-Base Zn(II) or Cd(II) complexes from a dynamic combinatorial library, Inorg. Chem. 40 (2001) 1591–1596.
[35] V.C. Da Silveira, J.S. Luz, C.C. Oliveira, I. Graziani, M.R. Ciriolo, A.M. Ferreira, Double-strand DNA cleavage induced by oxindole-Schiff base copper(II) complexes with potential antitumor activity, J. Inorg. Biochem. 102 (2008) 1090–1103.
[36] Y. Li, Z.Y. Yang, DNA binding affinity and antioxidative activity of copper(II) and zinc(II) complexes with a novel hesperetin Schiff base ligand, Inorg. Chim. Acta 362 (2009) 4823–4831.
[37] S. Kasselouri, A. Garoufis, A. Katehanakis, G. Kalkanis, S.P. Perlepes, N. Hadjiliadis, 1:1 Metal complexes of 2-(2′-pyridyl)quinoxaline, a ligand unexpectedly formed by the reaction between 2-acetylpyridine and 1,2-phenylenediamine, Inorg. Chim. Acta 207 (1993) 255–258.
[38] (a) M. Suresh, A. Das, New coumarin-based sensor molecule for magnesium and calcium ions, Tetrahedron Lett. 50 (2009) 5808–5812.
[39] (a) J. Hou, B. Liu, K. Li, K. Yu, M. Wu, X. Yu, Two birds with one stone: multifunctional and highly selective fluorescent probe for distinguishing Zn^{2+} from Cd^{2+} and selective recognition of sulfide anion, Talanta 116 (2013) 434–440;
(b) H. Wang, Y. Feng, S. Meng, A novel fluorescent sensor for Fe^{3+} and Cr^{3+} based on a calix[4] arene bearing two coumarin units, J. Chem. 36 (2012) 587–589, Res;
(c) J. Wu, R. Sheng, W. Liu, P. Wang, H. Zhang, J. Ma, Fluorescent sensors based on controllable conformational change for discrimination of Zn2+ over Cd2+, Tetrahedron 68 (2012) 5458–5463;
(d) N. Chattopadhyay, A. Mallick, S. Sengupta, Photophysical studies of 7-hydroxy-4-methyl-8-(4′-methylpiperazin-1′-yl) methylcoumarin: A new fluorescent chemosensor for zinc and nickel ions in water, J. Photoch. Photobio. A 177 (2006) 55–60.
[40] A. Liu, L. Yang, Z. Zhang, Z. Zhang, D. Xu, A novel rhodamine-based colorimetric and fluorescent sensor for the dual-channel detection of Cu^{2+} and Fe^{3+} in aqueous solutions, Dyes Pigm. 99 (2013) 472–479.
[41] J.Q. Ang, B.T.T. Nguyen, C.S. Toh, A dual K^+-Na^+ selective Prussian blue nanotubes sensor, Sens. Actuators B 157 (2011) 417–423.
[42] S. Goswami, S. Das, K. Aich, D. Sarkar, T.K. Mondal, Colorimetric as well as dual switching fluorescence 'turn on' chemosensors for exclusive recognition of Zn^{2+} and image in aqueous solution: experimental and theoretical studies, Tetrahedron Lett. 54 (2013) 6892–6896.
[43] S. Devaraj, Y.K. Tsui, C.Y. Chiang, Y.P. Yen, A new dual functional sensor: highly selective colorimetric chemosensor for Fe^{3+} and fluorescent sensor for Mg^{2+}, Spectrochim. Acta Part A Mol. Biomol. Spectrosc. 96 (2012) 594–599.
[44] O.G. Beltrán, B.K. Cassels, C. Pérez, N. Mena, M.T. Núñez, N.P. Martínez, P. Pavez, M.E. Aliaga, Coumarin-based fluorescent probes for dual recognition of copper(II) and iron(III) ions and their application in bio-imaging, Sensors 14 (2014) 1358–1371.
[45] T.S. Singh, P.C. Paul, H.A.R. Pramanik, Fluorescent chemosensor based on sensitive Schiff base for selective detection of Zn^{2+}, Spectrochim. Acta Part A: Mol. and Biol. Spec. 121 (2014) 520–526.
[46] A.D. Becke, Density-functional exchange-energy approximation with correct asymptotic behaviour, Phys. Rev. A 38 (1988) 3098–3100.
[47] C. Lee, W. Yang, R.G. Parr, Development of the colle-salvetti correlation-energy formula into a functional of the electron density, Phys. Rev. B 37 (1988) 785–789.
[48] P.C. Hariharan, J.A. Pople, The effect of d-functions on molecular orbital energies for hydrocarbons, Chem. Phys. Lett. 16 (1972) 217–219.
[49] Y. Xiang, A.J. Tong, A new rhodamine-Based chemosensor exhibiting selective Fe^{III}-Amplified fluorescence, Org. Lett. 8 (2006) 1549–1552.
[50] B. Virginia, G. Salvador, M.C. Ana, N.K. Maria, L. Ursula, M.E.M. Pedro, Luís E. Ochando, Margarita Parra, A new phenanthrene-based bis-oxime chemosensor for fe(III) and cr(III) discrimination, Tetrahedron 68 (2012) 4882–4887.
[51] V.C. Da Silveira, J.S. Luz, C.C. Oliveira, I. Graziani, M.R. Ciriolo, A.M. Ferreira, Double-strand DNA cleavage induced by oxindole-schiff base copper(II) complexes with potential antitumor activity, J. Inorg. Biochem. 102 (2008) 1090–1103.
[52] S. Moorthy, K.M. Amal, S. Sukdeb, E. Suresh, M. Amit, D.L. Rosa, Azine-based receptor for recognition of Hg^{2+} ion: crystallographic evidence and imaging application in live cells, Org. Lett. 12 (2010) 5406–5409.
[53] S.C. Yin, J. Zhang, H.K. Feng, Z.J. Zhao, L.W. Xu, H.Y. Qiu, Benzhong Tang, Zn^{2+}-selective fluorescent turn-on chemosensor based on terpyridine-substituted siloles, Dyes Pigm. 95 (2012) 174–179.
[54] J. Jayabharathi, V. Thanikachalam, K. Jayamoorthy, Effective fluorescent chemosensors for the detection of Zn^{2+} metal ion, Spectrochim. Acta A 95 (2012) 143–147.
[55] A. Reza, P. Maisam, T. Esmail, K. Hassan, G. Reza, Highly selective fluorescent recognition of Zn^{2+} based on naphthalene macrocyclic derivative, Spectrochim. Acta A 82 (2011) 200–204.

[56] T. Gunnlaugsson, T.C. Lee, R. Parkesh, Highly selective fluorescent chemosensors for cadmium in water, Tetrahedron 60 (2004) 11239–11249.
[57] C. Gao, X. Jin, X. Yan, P. An, Y. Zhang, L. Liu, H. Tian, W. Liu, X. Yao, Y. Tang, A small molecular fluorescent sensor for highly selectivity of zinc ion, Sens. Actuators B 176 (2013) 775–781.
[58] D. Zhang, M. Wang, M. Chai, X. Chen, Y. Ye, Y. Zhao, Three highly sensitive and selective colorimetric and off?on fluorescent chemosensors for Cu^{2+} in aqueous solution, Sens. Actuators B 168 (2012) 200–206.
[59] H.A. Benesi, J.H. Hildebrand, A spectrophotometric investigation of the interaction of iodine with aromatic hydrocarbons, J. Am. Chem. Soc. 71 (1949) 2703–2707.
[60] U. Fegade, A. Saini, S.K. Sahoo, N. Singh, R. Bendre, A. Kuwar, 2,2′-(hydrazine-1,2′ diylidenedimethylylidene) bis (6-isopropyl-3-methylphenol) based selective dual-channel chemosensor for Cu^{2+} in semi-aqueous media, RSC Adv. 4 (2014) 39639–39644.
[61] K.B. Kim, H. Kim, E.J. Song, S. Kim, I. Noh, C. Kim, A cap-type Schiff base acting as a fluorescence sensor for zinc(II) and a colorimetric sensor for iron(II), copper(II), and zinc(II) in aqueous media, Dalton Trans. 42 (2013) 16569–16577.
[62] A. Yoldas, F. Algi, An imidazo-phenanthroline scaffold enables both chromogenic Fe(II) and fluorogenic Zn(II) detection, RSC Adv. 5 (2015) 7868–7873.
[63] Y.S. Kim, G.J. Park, J.J. Lee, S.Y. Lee, S.Y. Lee, C. Kim, Multiple target chemosensor: a fluorescent sensor for Zn(II) and Al(III) and a chromogenic sensor for Fe(II) and Fe(III), RSC Adv. 5 (2015) 11229–11239.
[64] Y.W. Choi, G.J. Park, Y.J. Na, H.Y. Jo, S.A. Lee, G.R. You, C. Kim, A single schiff base molecule for recognizing multiple metal ions: a fluorescence sensor for Zn(II) and Al(III) and colorimetric sensor for Fe(II) and Fe(III), Sens. Actuators B 194 (2014) 343–352.
[65] A.J. Sanchez, B. Ortiz, V.O. Navarrete, J.C. Flores, N. Farfan, R. Santillan, A dual-model fluorescent Zn^{2+}/Cu^{2+} ions sensor with in-situ detection of $S^{2-}/(PO_4)^{-}$ and colorimetric detection of Fe^{2+} ion, Inorg. Chim. Acta 429 (2015) 243–251.
[66] A. Majumder, G.M. Rosair, A. Mallick, N. Chattopadhyay, S. Mitra, Synthesis structures and fluorescence of nickel, zinc and cadmium complexes with the N,N,O-tridentate Schiff base *N*-2-pyridylmethylidene-2-hydroxy-phenylamine, Polyhedron 25 (2006) 1753–1762.
[67] B. Kang, L. Weng, H. Liu, D. Wu, L. Huang, C. Lu, J. Cai, X. Chen, J.X. Lu, Syntheses structures, and properties of vanadium, cobalt, and nickel compounds with 2-mercaptophenol, Inorg. Chem. 29 (1990) 4873–4877.
[68] V.K. Gupta, N. Mergua, L.K. Kumawata, A.K. Singh, Selective naked-eye detection of magnesium (II) ions using a coumarin-derived fluorescent probe, Sens. Actuators B 207 (2015) 216–223.
[69] V.K. Gupta, A.K. Singh, L.K. Kumawat, Thiazole Schiff base turn-on fluorescent chemosensor for Al^{3+} ion, Sens. Actuators B 195 (2014) 98–108.
[70] V.K. Gupta, N. Mergu, L.K. Kumawat, A.K. Singh, A reversible fluorescence off-on-off sensor for sequential detection of aluminum and acetate/fluoride ions, Talanta 144 (2015) 80–89.
[71] H.G. Lee, K.B. Kim, G.J. Park, Y.J. Na, H.Y. Jo, S.A. Lee, C. Kim, An anthracene-based fluorescent sensor for sequential detection of zinc and copper ions, Inorg. Chem. Commun. 39 (2014) 61–65.
[72] V. Kumar, A. Kumar, U. Diwan, Shweta Ramesh, S.K. Srivastava, K.K. Upadhyay, Salicylideneimines as efficient dual channel emissive probes for Al^{3+}: harnessing ESIPT and ICT processes, Sens. Actuators B 207 (2015) 650–657.
[73] P.R. Bevington, Data Reduction and Error Analysis for the Physical Sciences, McGraw-Hill, Inc, New York, 1969.
[74] M. Sarkar, S. Banthia, A. Samanta, A highly selective 'off–on' fluorescence chemosensor for cr(III), Tetrahedron Lett. 47 (2006) 7575–7578.
[75] M.V. López, M.E. Vázquez, C. Gómez Reino, R. Pedrido, M.R. Bermejo, A metallo- supramolecular approach to a half-subtractor, New J. Chem. 32 (2008) 1473–1477.
[76] (a) A.P. de Silva, N.D. McClenaghan, Simultaneously multiply-Configurable or superposed molecular logic systems composed of ICT (Internal charge transfer) chromophores and fluorophores integrated with one- or two-Ion receptors, Chem. Eur. J. 8 (2002) 4935–4945.
[77] T.A. Koopmans, Über die zuordnung von wellenfunktionen und eigenwerten zu den einzelnen elektronen eines atoms, Physica 1 (1934) 104–113.

Biographies

Nayan Roy is a Ph. D student and pursuing research in the field of designing and synthesis of new chemical sensors and its application using different spectroscopic techniques under the supervision of Dr. T. Sanjoy Singh at Assam University, Silchar, Assam. He has completed his master degree in chemistry from Assam University, Silchar, Assam, India in 2012.

Abhijit Dutta is a Ph. D student and pursuing research in theoretical chemistry under the supervision of Dr. Paritosh Mondal at Assam University, Silchar, Assam. He has completed his master degree in chemistry from Assam University, Silchar, Assam, India in 2012.

Paritosh Mondal has a Ph.D. in theoretical chemistry obtained at Tezpur University, Assam, India, in 2009. Presently, he is holding the position of Associate Professor in the Department of Chemistry, Assam University, Silchar, India. His research interests include synthetic organic chemistry and theoretical chemistry.

Pradip C. Paul has a Ph.D. in inorganic chemistry obtained at North-Eastern Hill University, Shillong, India, in 1993. Presently, he is holding the position of Associate Professor in the Department of Chemistry, Assam University, Silchar, India. His research interests include synthetic inorganic chemistry, solution chemistry and liquid crystal.

T. Sanjoy Singh has a Ph.D. in physical chemistry and presently affiliated as an Assistant Professor in the Department of Chemistry, Assam University, Silchar, India. His current research interests include design and synthesis of chemosensors and its application, excited state charge transfer dynamics and protein-ligand interactions using fast and ultrafast time-resolved techniques.